AIAA JOURNAL
Vol. 48, No. 6, June 2010

# Boundary-Layer Transition on Broad Cones Rotating in an Imposed Axial Flow

S. J. Garrett*
*University of Leicester, Leicester, England LE1 2RH, United Kingdom*
and
Z. Hussain† and S. O. Stephen†
*University of Birmingham, Birmingham, England B15 2TT, United Kingdom*

DOI: 10.2514/1.J050021

**This paper presents stability analyses for the boundary-layer flow over broad cones (half-angle $\psi > 40°$) rotating in imposed axial flows. Preliminary convective instability analyses are presented that are based on the Orr—Sommerfeld equation for a variety of axial-flow speeds. The results are discussed in terms of the limited existing experimental data and previous stability analyses on related bodies. The results of an absolute-instability analysis are also presented which are intended to further those by Garrett and Peake [Garrett, S. J., and Peake, N., "The Absolute Instability of the Boundary Layer on a Rotating Cone," *European Journal of Mechanics, B/Fluids*, Vol. 263, 2007, pp. 344–353.] through the use of a more rigorous steady-flow formulation. Axial flow is seen to delay the onset of both convective and absolute instabilities.**

## Nomenclature

| | | |
|---|---|---|
| $k_\delta$ | = | modified disturbance wave number |
| $n$ | = | number of vortices |
| $P$ | = | steady pressure |
| $R_L$ | = | local Reynolds number |
| $r_\circ$ | = | local surface radius |
| $T_s$, $s$ | = | axial-flow parameters |
| $U$, $V$, $W$ | = | steady-flow velocity components in $x$, $\theta$, and $z$ directions |
| $U_\circ$ | = | local slip velocity |
| $\hat{u}$, $\hat{v}$, $\hat{w}$, $\hat{p}$ | = | perturbing quantities |
| $x$, $\theta$, $z$ | = | spatial variables in streamwise, azimuthal, and normal directions |
| $\alpha$, $\beta$ | = | disturbance wave number in $x$, and $\theta$ directions |
| $\gamma$, $\epsilon$ | = | disturbance frequency and wave angle |
| $\delta^\star$ | = | boundary-layer thickness (dimensional) |
| $\eta$, $\eta_1$ | = | transformed spatial variables in normal direction |
| $\phi_i$ | = | transformed perturbation variables |
| $\psi$ | = | cone half-angle |
| $\Omega^\star$ | = | angular velocity of rotation of cone (dimensional) |

## I. Introduction

THE rotating-disk boundary layer has long been used as a model for swept-wing flow because of the similarity between the basic-flow velocity profiles of the disk and the swept wing [1,2]. For this reason, research into the stability of rotating 3-D boundary-layer flows has been focused on the disk; very little theoretical work had been published on the boundary-layer flows over rotating spheres and cones before 2002. However, continuing developments in spinning projectiles, airfoils, aeroengines, and other industrial applications has led to the need to understand the onset of laminar–turbulent transition of the boundary-layer flows over rotating disks, spheres, and cones as objects in their own right.

For example, rotating spheres and cones are used as nose cones in aeroengine and spinning projectile applications. Here, laminar–turbulent transition within the boundary-layer flow over the nose cones can lead to significant increases in drag. For aeroengine applications this has negative implications for the fuel efficiency through increased noise and energy dissipation, and for projectile applications this has negative implications for control and accurate targeting. Understanding the stability of such boundary-layer flows and developing strategies to maintain laminar flow will lead to modifications in the design of these applications and enable significant cost savings. Furthermore, flows arising from rotating disks are present in types of chemical vapor deposition (CVD) reactors used for depositing thin films of optical and electrical materials on substrates in the electrochemical industry. Such reactors operate by forcing a carrier gas containing the reactive molecules onto the substrate held within a disklike support placed horizontally in the flow. The gas flow can be considered as a uniform axial flow incident on a rotating disk and it is desirable that the flow close to the substrate be laminar and free from instability to ensure uniform deposition. Although a large amount of literature exists on the theoretical and experimental study of the reactor-flow parameters [3–5], these are concerned with the changes in the laminar-flow profiles that can be achieved and the affect these have on deposition growth rates.

Although numerous flow-visualization studies [6–16] and recent theoretical studies [17–21] have been published on the boundary-layer flows over rotating spheres and cones, a complete understanding of the stability characteristics of such boundary layers with regard to these applications is still a long way off. This current paper is part of a series by the present authors [22,23] that considers the convective instability of the boundary-layer flow over a family of rotating cones (including the disk as the limiting half-angle), both in and out of an imposed axial flow. Particular emphasis is placed on the above applications. The series presents complementing numerical and asymptotic studies and commenced with an investigation into a family of cones rotating in an otherwise still fluid [22]. That study considered the stability of inviscid crossflow modes (type I) as well as modes which arise from a viscous-Coriolis force balance (type II). The influence of half-angle on the number and orientation of the spiral vortices was also examined, with comparisons drawn between the two distinct mathematical methods as well as with previous experimental studies. This was then followed by an investigation into the disk rotating in an imposed axial flow [23]. As we shall see in Sec. III.A, the mathematical formulation of the rotating-disk problem in axial flow is necessarily different from that for the rotating cone in axial flow, and this motivates separate

Received 22 June 2009; revision received 1 December 2009; accepted for publication 8 January 2010. 

*Department of Mathematics; s.garrett@mcs.le.ac.uk (Corresponding Author).
†School of Mathematics.

publication. This paper is different in structure from the previous two investigations in that it presents preliminary numerical results only; the asymptotic analysis is still in progress and will be published separately at a later date. In addition, this paper includes an investigation into the absolute instability of the boundary-layer flow, which is associated with the onset of turbulence [17–21,24,25].

Experimental observations of the transition over rotating cones have noted a distinction between the transition region on slender and broad cones. For example, experimental studies [7] of cones with slender half-angles rotating in still fluid show the existence of pairs of counter-rotating Görtler-type vortices. These arise from a dynamic instability induced by the centrifugal force of the flowfield. However, as the half-angle is increased beyond $\psi = 30°$, experimental results clearly show that the vortices change from pairs of counter-rotating vortices to corotating crossflow vortices as observed on rotating disks and spheres. The observed instability for slender cones therefore stems from an inherently different process. Indeed, Garrett et al. [22] hypothesize the existence of a viscous-mode dominated structure for slender cones ($\psi \leq 40°$), which leads to the onset of a centrifugal Görtler instability that is more dangerous than the usual type I and type II modes. The properties of the hypothesized centrifugal mode are further considered by Garrett [26].

Further evidence for different stability characteristics of slender and broad rotating cones is obtained from the recent experimental measurements for the onset of turbulence in otherwise still fluid at the University of Cambridge.[‡] The theoretical prediction for the onset of absolute instability by Garrett and Peake [20] is independent of half-angle and occurs at local Reynolds number $R \approx 2.5 \times 10^5$. Figure 1 shows the experimental results and we see that the onset of turbulence for the nonslender cone ($\psi = 60°$) is in good agreement with the predicted onset of absolute instability and is independent of rotation rate. However, the onset of turbulence for slender cones ($\psi = 30$ and $15°$) is well in advance of the predicted onset of absolute instability and dependent on the rotation rate. This observation clearly demonstrates that transition on slender cones is inconsistent with the onset of absolute instability. Indeed, Nickels and Bértenyi note different behavior in the turbulent intensity through transition in the case of the most slender cone which suggests a significantly different transition mechanism.

This paper focuses on the impact of axial flow on the stability of the boundary layers over broad rotating cones ($\psi > 40°$). An investigation into the hypothesized Görtler modes is underway and will be published at a later date.

With regard to similar theoretical studies, Kobayashi et al. [14,15] use local-linear-stability theory to predict the onset of spiral vortices in the boundary-layer flows over cones rotating in a uniform axial flow. Both papers consider a cone with a half-angle of $15°$ and predict the critical Reynolds number for the onset of the vortices, the vortex angle and the number of vortices as a function of an axial-flow parameter. The predictions are found to be qualitatively consistent with experimental measurements [15,16]. However, it is now clear that the transition mechanisms for slender cones are different for broad cones, which would explain why quantitative agreement was not obtained using their formulation.

Section IV of this paper is related to Garrett and Peake's [20] work on the absolute instability of the rotating-cone boundary layer in axial flow. The formulation of the laminar-flow profiles presented in this paper have been considerably improved and now lead to more physically relevant flows. The absolute-instability results contained here should therefore be considered as replacing those by Garrett and Peake, although their results for the cone rotating in an otherwise still fluid remain unchanged.

## II. Formulation

### A. Basic Flow

Consider a rigid cone of circular cross section and half-angle $\psi$ that is rotating about its axis of symmetry with angular velocity $\Omega^\star$. Note that an asterisk denotes a dimensional quantity in all that follows. The cone is placed in a fluid with an oncoming axial flow parallel to its axis of rotation. We choose the fixed orthogonal curvilinear coordinate system $(x^\star, \theta, z^\star)$ representing streamwise, azimuthal, and surface-normal variation, respectively, with the origin located at the apex of the cone. A diagram can be found in Fig. 1 of Garrett and Peake [20]. The local cross-sectional radius of the cone is $r_\circ^\star = x^\star \sin\psi$.

An appropriate coordinate transformation leads to the full Navier–Stokes equations in the coordinate system:

$$\frac{\partial U^\star}{\partial x^\star} + \frac{U^\star \sin\psi}{h^\star} + \frac{1}{h^\star}\frac{\partial V^\star}{\partial \theta} + \frac{\partial W^\star}{\partial z^\star} + \frac{W^\star \cos\psi}{h^\star} = 0 \tag{1}$$

$$\frac{\partial U^\star}{\partial t^\star} + U^\star\frac{\partial U^\star}{\partial x^\star} + \frac{V^\star}{h^\star}\frac{\partial U^\star}{\partial \theta} + W^\star\frac{\partial U^\star}{\partial z^\star} - \frac{V^{\star 2}\sin\psi}{h^\star} = -\frac{1}{\rho^\star}\frac{\partial P^\star}{\partial x^\star} + \nu^\star\left(\nabla^2 U^\star - \frac{2\sin\psi}{h^{\star 2}}\frac{\partial V^\star}{\partial \theta} - \frac{\sin\psi}{h^{\star 2}}(U^\star \sin\psi + W^\star\cos\psi)\right) \tag{2}$$

$$\frac{\partial V^\star}{\partial t^\star} + U^\star\frac{\partial V^\star}{\partial x^\star} + \frac{V^\star}{h^\star}\frac{\partial V^\star}{\partial \theta} + W^\star\frac{\partial V^\star}{\partial z^\star} + \frac{V^\star}{h^\star}(U^\star\sin\psi + W^\star\cos\psi) = -\frac{1}{h^\star\rho^\star}\frac{\partial P^\star}{\partial \theta} + \nu^\star\left(\nabla^2 V^\star + \frac{2}{h^{\star 2}} \times \left(\sin\psi\frac{\partial U^\star}{\partial \theta} + \cos\psi\frac{\partial W^\star}{\partial \theta}\right) - \frac{V^\star}{h^{\star 2}}\right) \tag{3}$$

$$\frac{\partial W^\star}{\partial t^\star} + U^\star\frac{\partial W^\star}{\partial x^\star} + \frac{V^\star}{h^\star}\frac{\partial W^\star}{\partial \theta} + W^\star\frac{\partial W^\star}{\partial z^\star} - \frac{V^{\star 2}\cos\psi}{h^\star} = -\frac{1}{\rho^\star}\frac{\partial P^\star}{\partial z^\star} + \nu^\star\left(\nabla^2 W^\star - \frac{2\cos\psi}{h^{\star 2}}\frac{\partial V^\star}{\partial \theta} - \frac{\cos\psi}{h^{\star 2}}(U^\star\sin\psi + W^\star\cos\psi)\right) \tag{4}$$

where

$$\nabla^{\star 2} = \frac{\partial^2}{\partial x^{\star 2}} + \frac{1}{h^{\star 2}}\frac{\partial^2}{\partial \theta^{\star}} + \frac{\partial}{\partial z^{\star 2}} + \frac{\sin\psi}{h^\star}\frac{\partial}{\partial x^\star} + \frac{\cos\psi}{h^\star}\frac{\partial}{\partial z^\star}$$

is the Laplacian operator and $h^\star = x^\star\sin\psi + z^\star\cos\psi$. Note that $\mathbf{U} = (U^\star, V^\star, W^\star)$ is the velocity flowfield and $P^\star$ is the fluid pressure.

At the edge of the boundary layer, the dimensional surface velocity distribution (i.e., the slip velocity) along the cone, $U_\circ^\star(x^\star)$, is given by the well-known potential-flow solution discussed by, for instance, Rosenhead [27] and Evans [28]. It takes the power-law form

$$U_\circ^\star(x^\star) = C^\star x^{\star m}$$

The value of the parameter $m$ is related to the cone half-angle (for instance, $m = 1$ when $\psi = 90°$ and $m = 0.1$ when $\psi = 27.72°$), and $C^\star$ is a scale factor determined by the freestream axial flow incident on the rotating cone. This inviscid solution is a good representation of the real slip velocity, since the separated boundary layer from the cone will tend to run parallel to the cone surface.

The appropriate boundary conditions are given by the slip and no-slip conditions at the edge of the boundary layer and the cone surface, respectively. These are represented as

$$U^\star = 0, \qquad V^\star = x^\star\Omega^\star\sin\psi, \qquad W^\star = 0 \quad \text{on } z^\star = 0$$

$$U^\star \to U_\circ^\star(x^\star), \qquad V^\star \to 0 \quad \text{as } z^\star \to \infty$$

The local axial-flow parameter $T_s$ is defined as

$$T_s = \frac{C^\star x^{\star m}}{x^\star\Omega^\star\sin\psi}$$

and is the ratio of the local slip velocity at $x^\star$ to the rotational speed of the cone surface at that location. It is important to note that in the case

[‡]Personal communication with T.B. Nickels and T. Bertényi, August 2007.

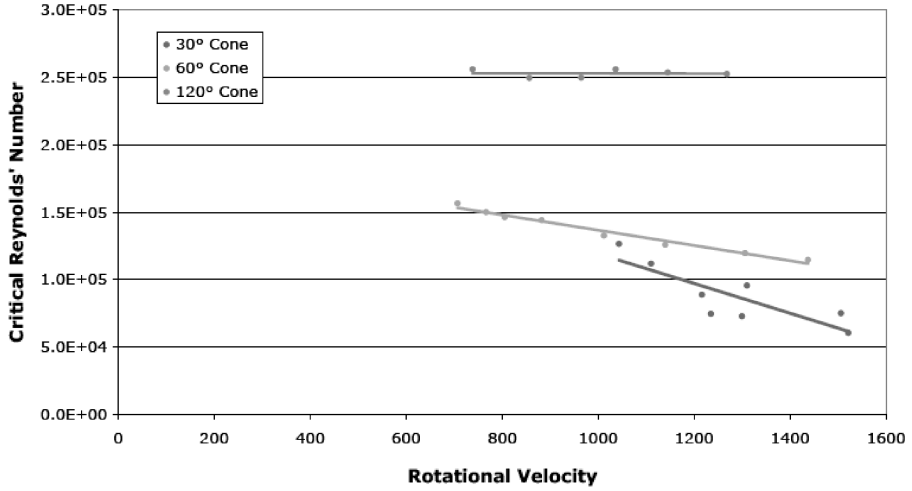


**Fig. 1 Experimental data for the onset of turbulence on rotating cones, uppermost plot is $\psi = 60°$ (cone angle $= 2\psi$).**

of $m \neq 1$ (i.e., $\psi \neq 90°$), $T_s$ is dependent on the streamwise coordinate. In effect, this causes the solution originally proposed by Garrett and Peake [20] to break down, as the equations governing the mean-flow are a system of partial differential equations in terms of the normal and streamwise coordinates. For this reason, we appeal to a different method of solution which is similar to that used by Koh and Price [29]. We make a similarity-type transformation yielding the boundary-layer equations in terms of the governing stream function. This is achieved by making a Mangler transformation on the governing equations. Suppose we define a new set of streamwise and surface-normal coordinates $\bar{x}^\star$ and $\bar{z}^\star$, respectively, and corresponding velocities $\bar{U}^\star$, $\bar{V}^\star$, and $\bar{W}^\star$, given by

$$\bar{x}^\star = \frac{1}{l^{\star 2}} \int_0^{x^\star} r_\circ^{\star 2}\, \mathrm{d}x^\star, \qquad \bar{z}^\star = \frac{r_\circ^\star}{l^\star} z^\star, \qquad \bar{U}^\star = U^\star$$
$$\bar{V}^\star = V^\star, \qquad \bar{W}^\star = \frac{l^\star}{r_\circ^\star}\left(W^\star + \frac{1}{r_\circ^\star}\frac{\mathrm{d}r_\circ^\star}{\mathrm{d}x^\star} z^\star U^\star\right) \tag{5}$$

where $l^\star$ is a typical length scale in the streamwise direction. The resulting boundary-layer equations may be derived in dimensional form using Eqs. (1–4) and transformation (5), which leads to

$$\frac{\partial \bar{U}^\star}{\partial \bar{x}^\star} + \frac{\partial \bar{W}^\star}{\partial \bar{z}^\star} = 0 \tag{6}$$

$$\bar{U}^\star \frac{\partial \bar{U}^\star}{\partial \bar{x}^\star} + \bar{W}^\star \frac{\partial \bar{U}^\star}{\partial \bar{z}^\star} - \frac{\bar{V}^{\star 2}}{3\bar{x}^\star} = \bar{U}_e^\star \frac{\partial \bar{U}_e^\star}{\partial \bar{x}^\star} + \nu^\star \frac{\partial^2 \bar{U}^\star}{\partial \bar{z}^{\star 2}} \tag{7}$$

$$\bar{U}^\star \frac{\partial \bar{V}^\star}{\partial \bar{x}^\star} + \bar{W}^\star \frac{\partial \bar{V}^\star}{\partial \bar{z}^\star} + \frac{\bar{U}^\star \bar{V}^\star}{3\bar{x}^\star} = \nu^\star \frac{\partial \bar{V}^\star}{\partial \bar{z}^{\star 2}} \tag{8}$$

where $\bar{U}_e^\star(\bar{x}^\star) = U_\circ^\star(x^\star) = C^\star x^{\star m}$. Applying the same transformations to the boundary conditions leads to

$$\bar{U}^\star = 0, \qquad \bar{V}^\star = \bar{V}_w = \omega^\star \bar{x}^{\star 1/3}, \qquad \bar{W}^\star = 0 \quad \text{on } \bar{z}^\star = 0$$
$$\bar{U}^\star \to \bar{U}_e^\star = \bar{C}^\star \bar{x}^{\star m/3}, \qquad \bar{V}^\star \to 0 \quad \text{as } \bar{z}^\star \to \infty$$

where

$$\bar{C}^\star = C^\star \left(\frac{3l^{\star 2}}{\sin^2\psi}\right)^{m/3} \quad \text{and} \quad \omega^\star = \Omega(3l^{\star 2}\sin\psi)^{1/3}$$

We then use the following similarity-type transformation which involves the stream function in the form

$$\bar{\psi} = \left(\frac{6\nu^\star \bar{x}^\star \bar{U}_e^\star}{m+3}\right)^{1/2} f(s, \eta_1), \qquad \bar{U}^\star = \frac{\partial \bar{\psi}}{\partial \bar{z}^\star}, \qquad \bar{W}^\star = -\frac{\partial \bar{\psi}}{\partial \bar{x}^\star}$$

where the parameters

$$s = \left(\frac{\bar{V}_w^\star}{\bar{U}_e^\star}\right)^2 = \left(\frac{\omega^\star}{\bar{C}^\star}\bar{x}^{\star \frac{1-m}{3}}\right)^2 \quad \text{and} \quad \eta_1 = \bar{z}^\star \left(\frac{m+3}{6}\frac{\bar{U}_e^\star}{\nu^\star \bar{x}^\star}\right)^{1/2}$$

define the transformed coordinates for the system. The $\eta_1$ coordinate represents the new surface-normal coordinate scaled on displacement thickness according to the new velocity scales, whereas the $s$ coordinate represents the ratio of rotational flow with respect to oncoming axial flow and is such that $s^{-1/2} = T_s$. The velocities can now be expressed as

$$\bar{U}^\star = \bar{U}_e^\star \frac{\partial f}{\partial \eta_1}(s, \eta_1), \bar{V}^\star = \bar{V}_w^\star g(s, \eta_1)$$
$$\bar{W}^\star = -\left(\frac{6}{m+3}\nu^\star \bar{x}^\star \bar{U}_e^\star\right)^{1/2}\left[\left(\frac{1}{2\bar{x}^\star} + \frac{1}{2\bar{U}_e^\star}\right) f + \frac{\mathrm{d}s}{\mathrm{d}\bar{x}^\star}\frac{\partial f}{\partial s} + \frac{\mathrm{d}\eta_1}{\mathrm{d}\bar{x}^\star}\frac{\partial f}{\partial \eta_1}\right]$$

These, together with Eqs. (6–8), lead to the governing partial differential equations that govern the laminar flow:

$$f''' + ff'' + \frac{2m}{m+3}(1 - f'^2) + \frac{2s}{m+3}\left[g^2 + 2(1-m)\left(f''\frac{\partial f}{\partial s} - f'\frac{\partial f'}{\partial s}\right)\right] = 0 \tag{9}$$

$$g'' + fg' - \frac{4}{m+3}f'g + \frac{4(1-m)s}{m+3}\left(g'\frac{\partial f}{\partial s} - f'\frac{\partial g}{\partial s}\right) = 0 \tag{10}$$

Note that a prime denotes differentiation with respect to $\eta_1$. Equations (9) and (10) are subject to the nondimensional boundary conditions:

$$f = 0, \qquad f' = 0, \qquad g = 1 \quad \text{on} \quad \eta_1 = 0$$
$$f' \to 1, \qquad g \to 0 \quad \text{as} \quad \eta_1 \to \infty \tag{11}$$

To solve the system of equations numerically, we decompose them into a fifth-order system of first-order partial differential equations. Solutions for $s = 0$ are obtained using a fourth-order Runge–Kutta integration method with a Newton–Raphson searching routine to iterate on the boundary conditions at infinity. These initial profiles are then integrated for nonzero $s$ to obtain profiles for varying $\eta_1$ and $s$ using the commercial NAG routine D03-DEF. The same routine has previously been used by Garrett [17] and Garrett and Peake [18,19] to obtain the basic flow over the rotating sphere both with and without an imposed axial flow.

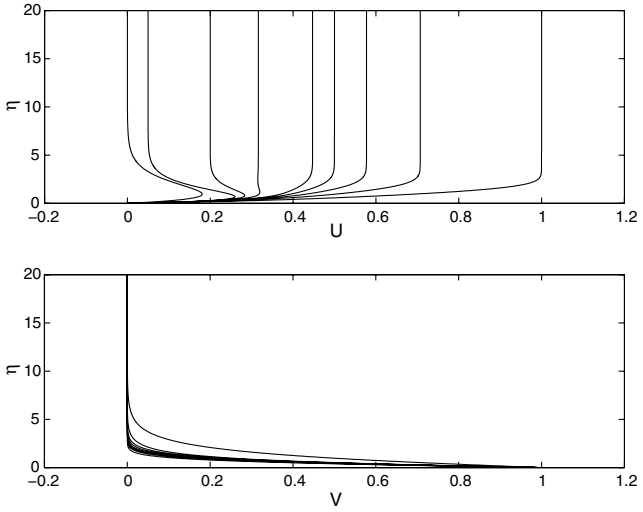


**Fig. 2 Steady-flow profiles for $\psi = 70°$ and $s = 1, 2, 3, 4, 5, 10, 25, 400, \infty$, right to left for $U$ and bottom to top for $V$.**

Convective and absolute instability are local concepts, and the analyses presented later will require the impulse response of the system to be determined within a parallel-flow-type approximation at a location $x^\star = x_s^\star$ along the surface of the cone. It is therefore appropriate to scale the steady velocities using the local surface velocity, $x_s^\star \Omega^\star \sin\psi$, as

$$U(\eta; x_s, \psi) = \frac{U^\star}{x_s^\star \Omega^\star \sin\psi}, \qquad V(\eta; x_s, \psi) = \frac{V^\star}{x_s^\star \Omega^\star \sin\psi}$$
$$W(\eta; x_s, \psi) = \frac{W^\star}{(\nu^\star \Omega^\star)^{1/2}}$$

where $\eta = z^\star/\delta^\star$ and $x_s = x_s^\star/\delta^\star$ are the nondimensional distances scaled on the boundary-layer thickness $\delta^\star = (\nu^\star/\Omega^\star)^{1/2}$. This is consistent with the numerical stability analyses presented in the literature [17–20,22,23,26]. Using this nondimensionalization, we note that

$$U = s^{-1/2} \frac{\partial f}{\partial \eta_1}(\eta_1, s), \qquad V = g(\eta_1, s)$$

which are expressible in terms of the nontransformed normal coordinate $\eta$ using the following coordinate stretching for a fixed axial-flow parameter $s$:

$$\eta_1 = \eta \left( \frac{m+3}{2s^{1/2}} \sin\psi \right)^{1/2}$$

It is not possible to reconstruct the $W$ component in an equivalent manner, and this has implications for the stability analysis presented in Sec. III.

Figure 2 shows the resulting $U$ and $V$ components of the steady flow for a variety of values of $s$. We see that as $s$ increases the rotational effect dominates over the oncoming axial flow and the streamwise profiles show an inflectional nature, overshooting before converging to the inviscid solution at the edge of the boundary layer.

Figure 3 shows two comparisons between the new profiles and those originally used in Garrett and Peake's analysis [20]. We note that the two are significantly different, with the new profiles suggesting a greater magnitude of streamwise flow close to the cone surface and the azimuthal flow experiencing a stronger shear effect. Such a difference in the steady-flow components will lead to an effective flow that has a stronger inflexion point which has implications for the predicted stability characteristics of the flow, and, for reasons discussed above, the new profiles are considered to be more accurate.

### B. Perturbation Equations

We use nondimensionalizing length, velocity, pressure, and time scales $\delta^\star$, $r_{\circ,s}^\star \Omega^\star$, $\rho^\star r_{\circ,s}^{\star 2} \Omega^{\star 2}$, and $\delta^\star/\Omega^\star r_{\circ,s}^\star$, respectively. This leads to the local Reynolds number $R_L$ at $x_s^\star$, where

$$R_L = \frac{x_s^\star \Omega^\star \delta^\star \sin\psi}{\nu^\star} = \frac{x_s^\star \sin\psi}{\delta^\star} = x_s \sin\psi = r_{\circ,s}$$

The governing disturbance equations at location $r_{\circ,s}$ are formed by perturbing the mean flow with quantities

$$(\hat{u}, \hat{v}, \hat{w}, \hat{p}) = (u(\eta), v(\eta), w(\eta), p(\eta)) \exp(i(\alpha x + \beta R_L \theta - \gamma t))$$

Physically, $\alpha$ is the disturbance wave number in the streamwise direction, $\beta$ is the wave number in the azimuthal direction, and $\gamma$ is the disturbance frequency. The quantities $\alpha$ and $\gamma$ are, in general, complex, as required by the spatiotemporal analysis presented later. In contrast, in order to enforce periodicity round the cone, $n = \beta R_L$ (identified as the number of vortices) must be interpreted at real integer values only. Note that these perturbing quantities are slightly different from those used by Garrett and Peake [20] through the removal of a factor of $\sin\psi$ multiplying $\alpha$. This is a minor adjustment and makes the formulation consistent with the more recent studies [22,23,26] by the present authors.

Substitution of the perturbing quantities into the general form of the Navier–Stokes equations (1–4) and nondimensionalizing leads to the linear perturbation equations. These may be written as a set of six first-order equations using the transformed variables[§]:

$$\phi_1 = \bar{\alpha} u + \beta v, \qquad \phi_2 = \bar{\alpha} D u + \beta D v, \qquad \phi_3 = w, \qquad \phi_4 = p$$
$$\phi_5 = \bar{\alpha} v - \beta u, \qquad \phi_6 = \bar{\alpha} D v - \beta D u$$

where $D$ represents differentiation with respect to $\eta$ and $\bar{\alpha} = \alpha - [i \sin\psi/R]_s$. These equations are

$$D\phi_1 = \phi_2 \tag{12}$$

$$\left[\frac{D\phi_2}{R_L}\right]_V = \frac{1}{R_L}([\alpha^2+\beta^2]_S + iR_L(\bar{\alpha}U + \beta V - \gamma))\phi_1 + \left[\frac{W\phi_2}{R_L}\right]_S + \left[\frac{V}{R_L}\beta\cos\psi + \bar{\alpha}DU + \beta DV\right]\phi_3 + i(\alpha\bar{\alpha} + \beta^2)\phi_4 - \left[\frac{V\sin\psi}{R_L}\phi_5\right]_S + \left[\left(\bar{\alpha}\frac{\partial U}{\partial x} + \beta\frac{\partial V}{\partial x}\right)u - \frac{\sin\psi}{R_L}(\bar{\alpha}V - \beta U)v\right]_S \tag{13}$$

$$D\phi_3 = -i\phi_1 - \left[\frac{\phi_3\cos\psi}{R_L}\right]_S \tag{14}$$

$$D\phi_4 = \left[\frac{iW\phi_1}{R_L}\right]_S - \left[\frac{i\phi_2}{R_L}\right]_V - \frac{1}{R_L}([\alpha^2+\beta^2]_S + iR_L(\alpha U + \beta V - \gamma) + DW_S)\phi_3 \tag{15}$$

$$D\phi_5 = \phi_6 \tag{16}$$

$$\left[\frac{D\phi_6}{R_L}\right]_S = \frac{1}{R_L}([\alpha^2+\beta^2]_V + iR_L(\bar{\alpha}U + \beta V - \gamma))\phi_5 + \left[\frac{W\phi_6}{R_L}\right]_S + \left[\frac{V}{R_L}\bar{\alpha}\cos\psi + \bar{\alpha}DV - \beta DU\right]\phi_3 + \left[\frac{\beta\sin\psi}{R_L}\phi_4\right]_S + \left[\frac{V\sin\psi}{R_L}\phi_1\right]_S + \left[\left(\bar{\alpha}\frac{\partial V}{\partial x} - \beta\frac{\partial U}{\partial x}\right)u + \frac{\sin\psi}{R_L}(\bar{\alpha}U + \beta V)v\right]_S \tag{17}$$

[§]A typographical error has been noticed in [20] in the definition of $\phi_{5,6}$.

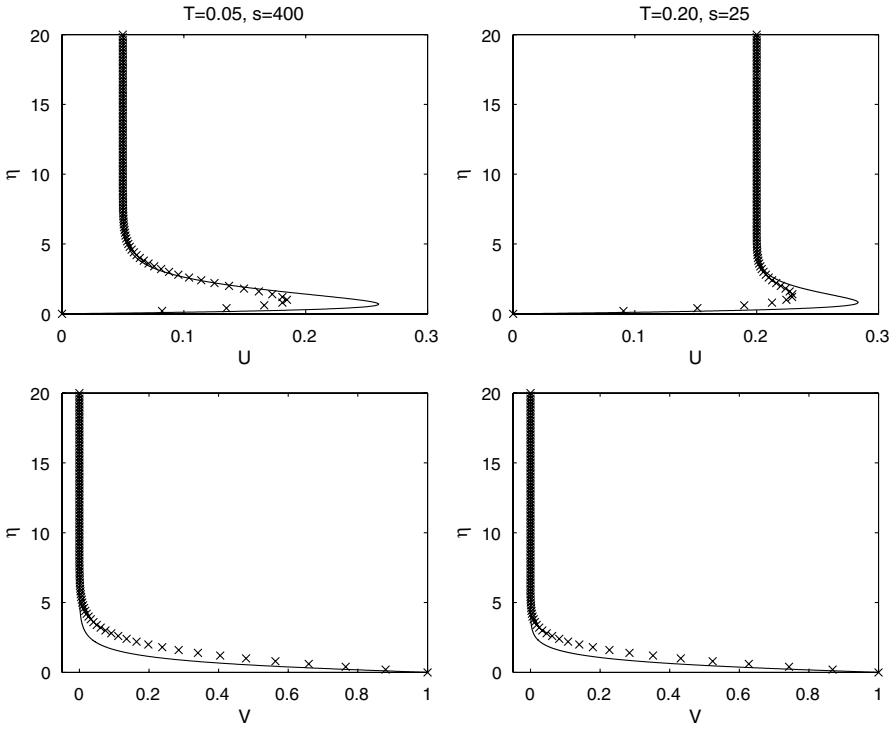


**Fig. 3 Steady-flow profiles for $\psi = 70°$ and $s = 400$ and 25 computed using the methods present here (solid line) and by Garrett and Peake [20] ($x$).**

where the subscripts $V$ and $S$ indicate which of the $O(R_L^{-1})$ terms arise from viscous and streamline-curvature effects, respectively. Note that the perturbation quantities $u$ and $v$ appear explicitly in (12–17), but can be expressed in terms of $\phi_1$ and $\phi_5$ via

$$u = \frac{\bar{\alpha}\phi_1 - \beta\phi_5}{\bar{\alpha}^2 + \beta^2}, \qquad v = \frac{\bar{\alpha}\phi_5 + \beta\phi_1}{\bar{\alpha}^2 + \beta^2}$$

This formulation is such that the axial-flow parameter $s$ only appears in the steady-flow equations. Equations (12–17) reduce to Lingwood's [24] perturbation equations for the rotating disk (in an appropriate frame of reference) when $\psi = 90°$ and the basic-flow components are given by von Kármán's similarity solution. The perturbation equations differ from those stated by Garrett and Peake [20] due to the different definition of $\alpha$ and the acknowledgment that the basic-flow components are functions of both $\eta$ and $x$.

In this preliminary investigation we present a study of the Orr–Sommerfeld (OS) equation for the cone rotating in imposed axial flows. The governing fourth-order perturbation equation is obtained by neglecting streamline-curvature effects in the full-perturbation equations above. This leads to

$$[i(D^2 - k^2)^2 + R_L(\alpha U + \beta V - \gamma)(D^2 - \gamma^2) - R_L(\alpha D^2 U + \beta D^2 V)]\phi_3 = 0 \tag{18}$$

where $k^2 = \alpha^2 + \beta^2$ is the effective wave number of the disturbance.

Analysis of the OS equation greatly simplifies the investigation as it removes the requirement for the normal velocity component $W$ and derivatives with respect to the streamwise direction. This simplification is necessary as we are unable to reconstruct the $W$ component in the form required by the full-perturbation equations. Although it would be possible to reform the perturbation equations using the Mangler transformation and incorporate the transformed steady-flow profiles directly, we have chosen to maintain the formulation in order to facilitate comparisons with the previous body of work [17–20,22–24,26,30]. These previous studies have shown that although the predicted onset of instability is underestimated and the relative importance of the streamline-curvature mode (type II) is unable to be predicted, analysis of the OS equation leads to qualitatively correct predictions which increase in numerical accuracy as $R_L \to \infty$. This is further discussed in Sec. III.

Equations (12–17) use a parallel-flow-type approximation in which we ignore variation in the local Reynolds number $R_L$ with local surface cross-sectional radius and assume that $\eta/r_\circ \ll 1$. This involves replacing the variable $r_\circ + \eta\cos\psi$, which appears in the coefficients of the perturbation equations, by $R_L$. The resulting stability results are then strictly local, with location $R_L = r_{\circ,s}$ appearing as a parameter. The assumption $R_L \gg 1$ (equivalent to $\delta^\star \ll x^\star$) necessarily prohibits analysis close to the apex in which $R_L = O(1)$. The implications of this approximation are discussed in Sec. V.

## III. Convective Instability

In this section we solve the eigenvalue problem defined by the OS equation (18), with the homogeneous boundary conditions

$$\phi_i = 0 \quad \text{on} \quad \eta = 0, \qquad \phi_i \to 0 \quad \text{as} \quad \eta \to \infty \tag{19}$$

where $i = 1, 2, \ldots, 4$. This eigenvalue problem will be solved for certain combinations of values of $\alpha$, $\beta$ and $\gamma$ at each Reynolds number, $R_L$ for a particular half-angle. From these we form the dispersion relation, $D(\alpha, \beta, \gamma; R_L, \psi) = 0$, with the aim of studying the occurrence of convective instabilities. This allows a discussion of the spatial branches of the dispersion relation before we study their pinching in the absolute-instability analysis of Sec. IV. In each analysis the branches were calculated using a fourth-order Runge–Kutta integrator with Gram–Schmidt orthonormalization and a Newton–Raphson linear search procedure.

Since we are supposing here that the flow is not absolutely unstable, it follows that in the Briggs–Bers procedure we can reduce the imaginary part of the frequency down to zero, so that $\gamma_i = 0$. To produce the neutral curves for convective instability a number of approaches can be taken in this stationary frame of reference. One approach is to insist that the vortices rotate at some fixed multiple of the cone surface velocity, thereby fixing the ratio $\gamma_r/\beta$, and then $\alpha$ and $\beta$ are calculated using a spatial analysis. This is the approach taken here. In particular, we explicitly assume that the vortices rotate with the surface of the cone (i.e., are *stationary*) so that $\gamma_i = \beta$, which is consistent with experimental observations discussed in Sec. I. As discussed by Corke and Knasiak [31], traveling modes can dominate on a highly polished rotating disk, and this is also likely to be the case

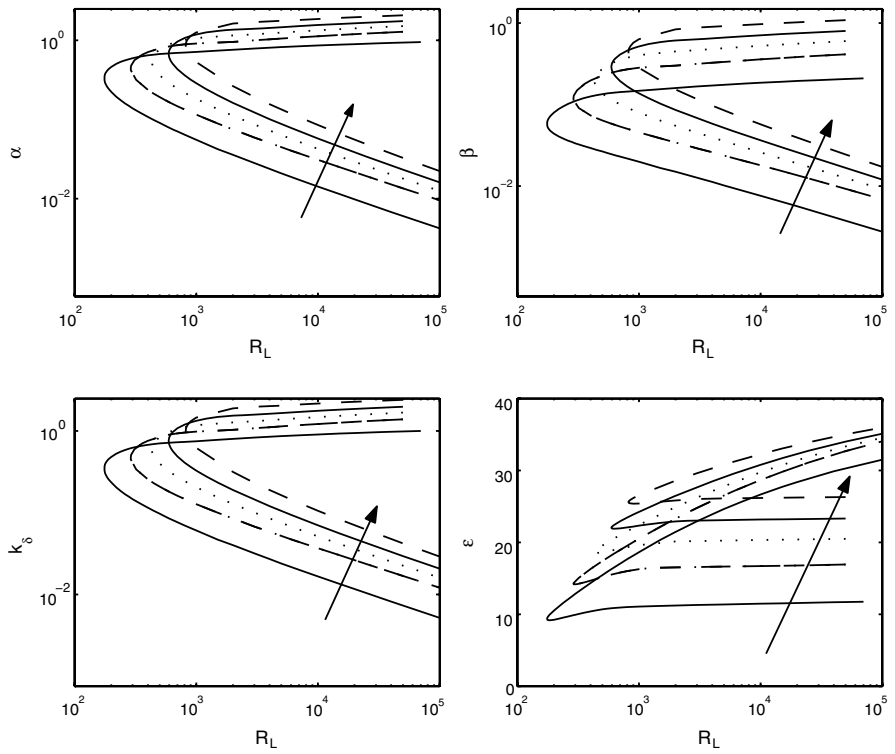


**Fig. 4 Orr–Sommerfeld neutral curves for convective instability of stationary vortices for $\psi = 70°$ with $s = \infty$, 400, 25, 10, and 5; arrow indicates direction of decreasing $s$ (i.e., increasing axial flow).**

over a highly polished broad rotating cone. However, we are particularly interested in practical engineering applications, in which highly polished surfaces will not be found.

### A. Cone Rotating in Otherwise Still Fluid and Disk Rotating in Axial Flow

In [22] the present authors give the convective instability analysis for a family of cones rotating in an otherwise still fluid. An appropriate version of the full system of perturbation equations (12–17) is used, and both numerical and asymptotic approaches are taken. Furthermore, the equivalent analysis for a disk placed in an enforced axial flow is contained in [23]. The interested reader is therefore referred to those publications in the limiting cases of $s \to \infty$ for all $\psi$ and $\psi = 90°$ for all $s$. We now proceed to present an analysis for nonzero axial flow incident on rotating cones (i.e., finite $s$ and $\psi \neq 90°$).

### B. Cone Rotating in Uniform Axial Flow

One spatial branch was found to determine the convective instability characteristics in the OS analysis for each half-angle considered for each axial-flow rate. This branch arises from the crossflow (type I) instability mode and is identical to that discussed in [18,19,30]. It is known that this mode arises from the inflectional nature of the streamwise mean velocity component $U$. Previous investigations of related boundary layers have also noted the appearance of a streamline-curvature (type II) instability mode. This corresponds to a centrifugal instability associated with the way in which the outer-flow streamlines are curved by an $O(R_L^{-1})$ amount close to the outer edge of the boundary layer. However, since streamline-curvature effects have been removed in this preliminary investigation of the OS equation, the type II mode does not arise.

Figure 4 shows the neutral curves in the $(R_L, \alpha_r)$, $(R_L, \beta)$, $(R_L, k_\delta)$, and $(R_L, \epsilon)$ planes for $\psi = 70°$ for a variety of values of $s$. Note that $k_\delta = \sqrt{\alpha^2 + \beta^2}/\sin\psi$ is the modified wave number and $\epsilon = \arctan(\beta \sin\psi/\alpha_r)$ is the modified wave angle of the disturbances. Although the introduction of the factor $\sin\psi$ appears arbitrary here, it arises from the formulation of the asymptotic study (not presented here) and enables comparison with the previous numerical and asymptotic investigations [22,23] (the interested reader is referred to those publications for more details). The neutral curves are determined by setting $\gamma_i = 0$ (i.e., a neutral disturbance) and $\gamma_r = \beta$ (i.e., to guarantee stationary disturbances), and for each $R_L$ the dispersion relation is then solved to return a pair of values $(\alpha_r, \beta)$ for each neutral mode. As can be seen in Fig. 4, the value of $\beta$ varies continuously, although only values of $\beta$ are allowed, of course, such that $n$ is an integer. Inside each loop of the neutral curves, the flow is convectively unstable.

Figure 4 clearly demonstrates that axial flow has a stabilizing effect on the rotating-cone boundary layer by increasing the critical Reynolds number for the onset of instability. It is also clear that the range of wave angles that the spiral vortices are predicted to exist is narrowed with increased axial flow. Table 1 lists the critical values of $R_L, x_L = R_L/\sin\psi$, vortex angle and number of vortices at the onset

**Table 1 Critical parameters at the onset of convective instability for a range of axial-flow rates**

| | | $\psi = 70°$ | | | | $\psi = 50°$ | | | |
|---|---|---|---|---|---|---|---|---|---|
| $s$ | $T_s$ | $R_L$ | $x_L$ | $\epsilon$ | $n$ | $R_L$ | $x_L$ | $\epsilon$ | $n$ |
| $\infty$ | 0 | 175.5 | 186.8 | 9.2° | ∼10 | 158.5 | 206.9 | 7.6° | ∼8 |
| 10,000 | 0.01 | 265.6 | 282.6 | 13.2° | ∼27 | 272.1 | 355.2 | 10.6° | ∼29 |
| 400 | 0.050 | 289.4 | 308.0 | 14.2° | ∼34 | 296.2 | 386.7 | 11.5° | ∼36 |
| 25 | 0.200 | 432.1 | 459.8 | 18.6° | ∼85 | 433.6 | 566.0 | 12.1° | ∼88 |
| 10 | 0.316 | 594.1 | 632.2 | 22.0° | ∼170 | 588.1 | 767.7 | 18.0° | ∼175 |
| 5 | 0.447 | 819.7 | 872.3 | 25.6° | ∼360 | 803.1 | 1048.4 | 21.0° | ∼360 |

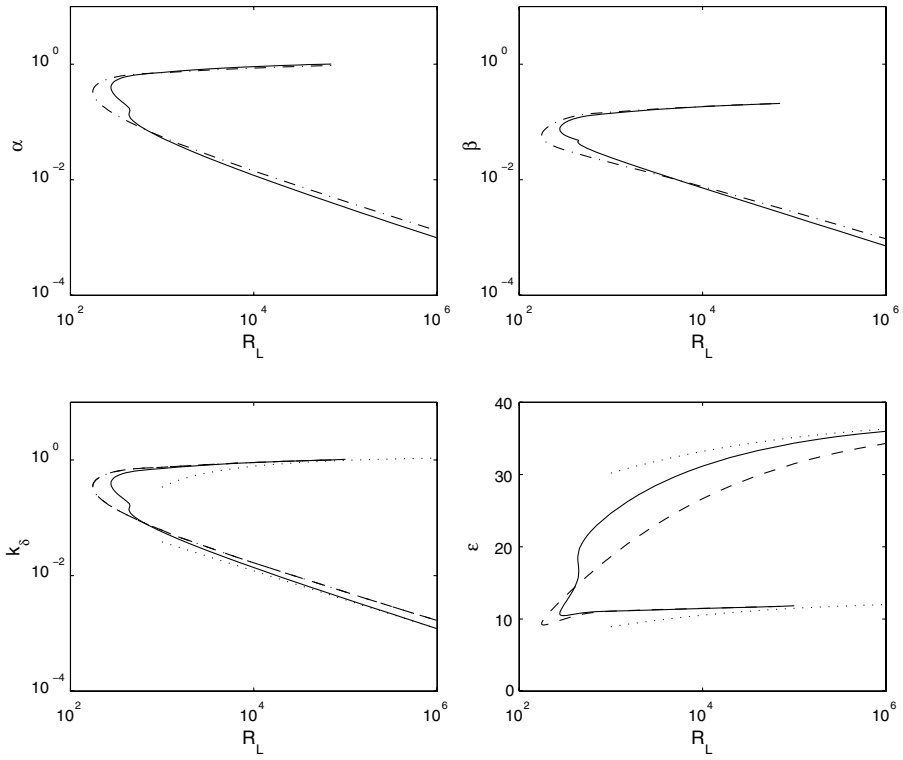


**Fig. 5 Comparison of Orr–Sommerfeld neutral curves (dotted–dashed line) with full-perturbation-system neutral curves (solid line) and the asymptotics (dotted line) for the convective instability of stationary disturbances over a cone rotating in otherwise still fluid ($s \to \infty$) ($\psi = 70°$).**

of convective instability at each axial flow rate and half-angle studied using the Orr–Sommerfeld formulation.

Unfortunately, experimental results [8,16] for rotating cones in axial flow exist only for $\psi = 15°$. It is therefore possible to compare our calculations for $\psi = 70$ and 50° only qualitatively with these studies. Agreement is found with the general trend that axial flow delays the onset of spiral vortices and increases their wave angle.

To compare the onset of convective instability at each $s$ between both values of $\psi$, it is sensible to use $x_L = R_L / \sin\psi$ (the nondimensional distance along the cone surface). Table 1 shows that the onset of convective instability occurs further along the 50° one than the 70° cone for each value of $T_s$. However, it is clear from the definition of the axial-flow parameter that equal values of $T_s$ for both values of $\psi$ does not translate as equal incident axial-flow rates. This is due to the appearance of $m$, which depends on $\psi$. Care must therefore be taken in making such comparisons. The interpretation of such comparisons is discussed further by Garrett [17] and Garrett and Peake [20]. We are able to conclude that the critical values of the 50° cone appear to be more sensitive to the values of $T_s$ than those of the 70° cone.

To discuss the relative importance of the type I and type II modes of instability it is necessary to consider the full-perturbation system of equations (12–17), which is not done here. For the related boundary-layer flows over rotating spheres and disks, Garrett and Peake [19] and the present authors [22] find that increased axial flow increases the importance of the type II (streamline-curvature) mode until it becomes the most dangerous below a certain value of $s$. The suggestion that increased axial flow would emphasize the streamline-curvature mode is also sensible in this geometry. In particular, Fig. 2 shows that axial flow increases the amount of fluid entrained into the boundary layer, which would clearly lead to more streamline curvature. It is also expected that this will occur on rotating cones of other half-angles. Physically, it is suggested that axial flow effectively sweeps any instabilities arising from, say, surface roughness further downstream, causing the location of transition to retreat downstream also. Therefore, axial flow has a stabilizing effect on convective instabilities.

Figure 5 demonstrates the implications of using the OS equation (18) instead of the full-perturbation equations (12–17) for a cone with $\psi = 70°$ rotating in an otherwise still fluid. This is done by plotting neutral curves as in Fig. 4, but calculated from each system of equations. In each plot we see a marked difference in the behavior close to the critical value of $R_L$, most notably in that the two-lobed structure does not exist in the OS analysis, but also that the critical values of $R_L$ are lower in the OS analysis. As $R_L$ increases, excellent agreement is obtained in the upper-branch calculations in the $(R_L, \alpha_r)$, $(R_L, \beta)$, and $(R_L, k_\delta)$ planes and good agreement is obtained in the lower branches. In the $(R_L, \epsilon)$ plane excellent agreement is obtained in the lower branch (which corresponds to the upper branch of the other plots) but the discrepancy in the predicted upper-branch wave angle is more noticeable (although this is partly to do with the log scalings used in the other plots). The wave angle and wave number plots also show the comparison with the

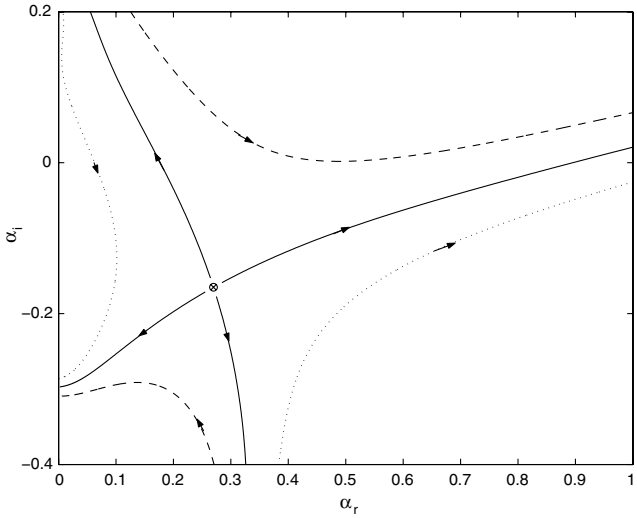


**Fig. 6 Branches of type I and type III for $\psi = 70°$ and $s = 10,000$ for $R_L = 3000$, $\beta = 0.26$, $\gamma_i = 0.0025$ (solid line), $\gamma_i = 0.01$ (dashed line), and $\gamma_i = -0.005$ (dotted line); arrows indicate direction of increasing $\gamma_r$ and the cross indicates the pinch point.**

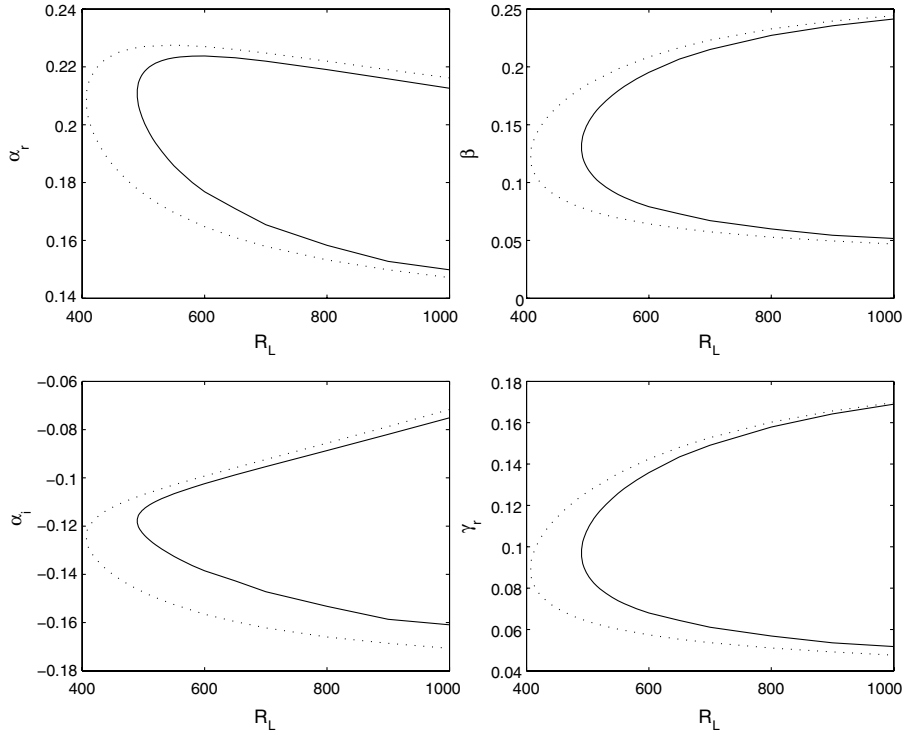


**Fig. 7 Comparison of Orr–Sommerfeld neutral curves (dotted line) with full-perturbation-system neutral curves (solid line) for absolute instability of a cone rotating in otherwise still fluid ($s \to \infty$) for $\psi = 70°$.**

asymptotic predictions. Figure 5 therefore demonstrates that the results from this preliminary OS analysis are expected to be quantitatively close to those arising from the full system. However, the relative importance of the type I and type II modes (as determined by the two-lobed structure) cannot be investigated under the OS formulation, as mentioned above. Both the full-system numerics and the asymptotic plots in Fig. 5 are by the present authors [22], in which a full description can be found. For comparison with the data in Table 1, the critical parameters at the onset of convective instability arising from the full system of equations for $\psi = 70°$ and $s = \infty$ are $R_L \approx 277, \epsilon = 11°$, and $n \sim 21$, and for $\psi = 50°$ and $s = \infty$ they are $R_L \approx 249, \epsilon = 9°$, and $n \sim 16$.

## IV. Absolute Instability

We now solve the OS eigenvalue problem with the aim of studying the occurrence of absolute instability. The Briggs–Bers method is used to detect an absolutely unstable response to the initial

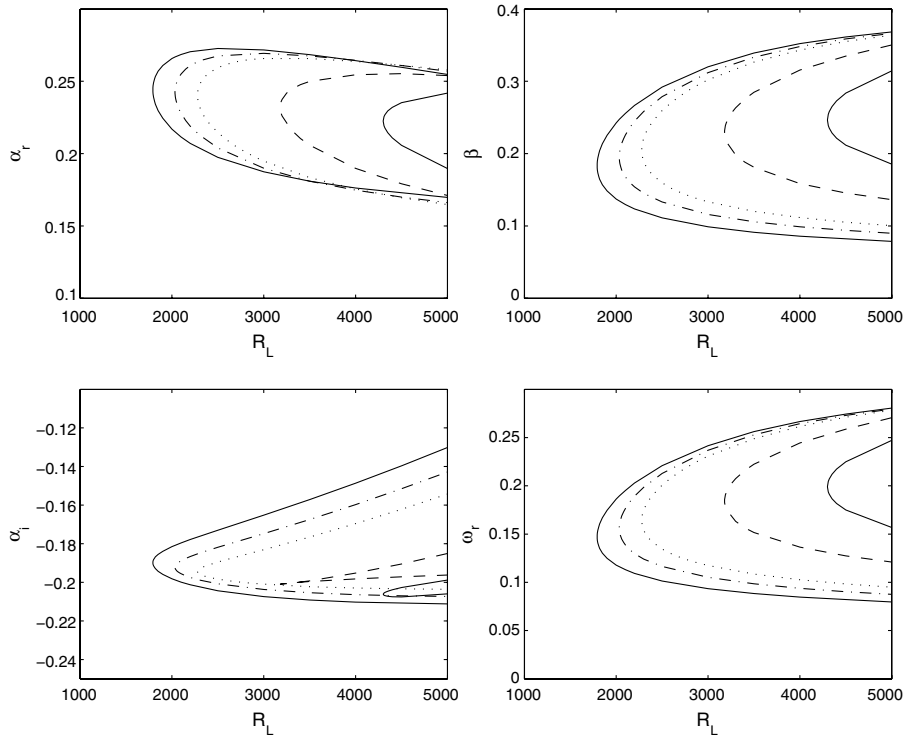


**Fig. 8 Orr–Sommerfeld neutral curves for absolute instability of a cone rotating in otherwise still fluid ($s \to \infty$) for $\psi = 70°$. Curves are shown for $s = 10,000, 1000, 400, 100$, and 50 from left to right (i.e., increasing axial flow).**

perturbation of the form $\delta(r - r_s)\delta(t)e^{i\beta\theta}$. For absolute instability to occur we need to locate a pinch point $(\alpha^\circ, \gamma^\circ)$, formed by the coalescence between two spatial branches which originate from distinct half-$\alpha$ planes when $\gamma_i$ is sufficiently large and positive. The flow is then absolutely unstable if $\gamma_i > 0$ at the pinch point and is otherwise, at worst, convectively unstable.

A pinch point has indeed been found for each half-angle $\psi$ and flow parameter $s$, which is unstable for sufficiently large $R_L$. The pinch for a particular set of parameter values is shown in Fig. 6, in which the characteristic exchange of branches can be seen. This pinching behavior is consistent with that previously found on related geometries [17–21,24,25]. By monitoring the behavior of the two spatial branches as the Reynolds number is varied, it is possible to determine the critical value of $R_L$ for the onset of absolute instability. As Lingwood [24] and Garrett and Peake [18,19] have demonstrated with previous analyses of the OS/full system of perturbation equations, the pinch is formed by the coalescence of two branches which are inviscid in origin. One is the convectively unstable type I branch and the other is a convectively stable branch (typically denoted as type III). Existence of a pinch in this current OS analysis would therefore demonstrate that the rotating-cone boundary layer is absolutely unstable in axial flow, although the predicted onset will be quantitatively different from that predicted by the more accurate full-perturbation system. As with the convective instability case, the extent of the discrepancy can be judged by plotting neutral curves for absolute instability for a cone rotating in otherwise still fluid. Figure 7 demonstrates the implications of using the OS Eq. (18) instead of the full-perturbation equations (12–17) for a cone with $\psi = 70^\circ$ rotating in an otherwise still fluid in terms of the $(R_L, \alpha_r)$, $(R_L, \alpha_i)$, $(R_L, \beta)$, and $(R_L, \gamma_r)$ planes.

### A. Cone Rotating in Otherwise Still Fluid and Disk Rotating in Axial Flow

Garrett and Peake [20] give the results of absolute-instability analyses for a family of cones rotating in a range of axial flows. They use the full system of perturbation equations. As discussed above, this current paper uses more accurate basic-flow profiles for nonzero axial flow imposed on rotating cones and so the results are intended to replace those previously published. However, the basic flows obtained using the methods detailed in Sec. II.A are identical to those obtained previously for zero axial flow ($T_s = 0$, $s \to \infty$) for all $\psi$ and for $T_s \neq 0$ when $\psi = 90^\circ$. The existing results for these cases are therefore unchanged and the interested reader is referred to Garrett and Peake [20].

### B. Cone Rotating in Uniform Axial Flow

Figure 8 shows neutral curves for absolute instability when $\psi = 70^\circ$ in terms of the $(R_L, \alpha_r)$, $(R_L, \alpha_i)$, $(R_L, \beta)$, and $(R_L, \gamma_r)$ planes at $s = 10,000$, 1000, 400, 100, and 50. The most striking feature of this figure is the sensitivity of absolute instability to axial flow. For example, the onset of convective instability is delayed from $R_L \approx 176$ to 289 as the imposed axial flow is increased from $s = \infty$ ($T_s = 0$) to $s = 400$ ($T_s = 0.05$); this represents an increase of around 60%. However, the onset of absolute instability is increased from $R_L \approx 407$ to 2279 over the same range of $s$; this is an increase of around 460%. For this reason, the figure shows the neutral curves over a much shorter range of axial-flow parameters.

**Table 2 Critical parameters at the onset of absolute instability for a range of axial-flow rates**

| | | $\psi = 70^\circ$ | | $\psi = 50^\circ$ | |
|---|---|---|---|---|---|
| $s$ | $T_s$ | $R_L$ | $x_L$ | $R_L$ | $x_L$ |
| $\infty$ | 0 | 406.4 | 432.5 | 368.0 | 480.4 |
| 10,000 | 0.010 | 1792.9 | 1908.0 | 1669.4 | 2179.2 |
| 1000 | 0.032 | 2033.9 | 2164.4 | 1891.2 | 2468.8 |
| 400 | 0.050 | 2278.8 | 2425.0 | 2116.2 | 2762.5 |
| 100 | 0.100 | 3180.5 | 3384.6 | 2947.3 | 3847.4 |
| 50 | 0.141 | 4301.0 | 4577.0 | 3982.3 | 5198.5 |
| 25 | 0.200 | 6882.5 | 7324.2 | 6372.4 | 8318.6 |

Table 2 lists the critical values of $R_L$ and $x_L$ for the onset of absolute instability at each axial flow rate and half-angle studied using the Orr–Sommerfeld formulation. For comparison, the results obtained from the full-perturbation system for cones rotating in zero axial flow are $R_L \approx 490$ for $\psi = 70^\circ$ and $R_L \approx 441$ for $\psi = 50^\circ$. As with $\psi = 70^\circ$, the onset of absolute instability over the 50° cone is seen to be very sensitive to axial flow. As with the onset of convective instability, the delayed onset of absolute instability with $T_s$ for $\psi = 50^\circ$ is more sensitive than for $\psi = 70^\circ$.

## V. Conclusions

In this paper we have used an Orr–Sommerfeld analysis to show that the boundary layer over a broad cone ($\psi > 40^\circ$) rotating in an imposed axial flow is both convectively and absolutely unstable. Use of the Orr–Sommerfeld system, which neglects the normal component of the steady flow, has been necessary from our desire to present a stability analysis consistent with our previous analyses but using an alternative formulation for the steady-flow profiles. The onsets of both instabilities are delayed with increased $T_s$ (i.e., decreased $s$) and the critical position for onset (as measured along the surface of the cone) is delayed with decreased $\psi$.

Figure 3 demonstrates that the steady-flow profiles used here are significantly different from those used in Garrett and Peake's [20] related analyses for nonzero axial flow onto rotating cones (with $\psi \neq 90^\circ$). Garrett and Peake use the full system of perturbation equations in their analysis and a direct quantitative comparison between the results cannot therefore be made. However, it is clear that the use of the alternative (and more accurate) profiles developed here has made a significant difference to predicted stability properties of the flow. In particular, the onset of absolute instability is seen to be far more sensitive to axial flow than originally predicted by Garrett and Peake. It is acknowledged that a compromise has been made in which a less representative form of the stability equations has been used in order to use more accurate steady-flow profiles, however, the Orr–Sommerfeld results are known to envelope those arising from the full system of equations and so all qualitative conclusions are expected to hold. For this reason, these results are intended to replace those given by Garrett and Peake in all cases in which $\psi \neq 90^\circ$ and $T_s \neq 0$.

We have made use of a parallel-flow-type approximation by assuming that factors $1 + \eta \cos\psi / R_L$ can be replaced by unity. We are careful to point out that this approximation would imply that the resulting perturbation equations are not consistent to $\mathcal{O}(R_L^{-1})$, the same order as the viscous and streamline-curvature effects. Therefore, whether using the Orr–Sommerfeld Eq. (18) or the full-perturbation equations (12–17), the solutions cannot be justified rigorously at finite $R_L$. It is the authors' opinion that this approximation will not affect the conclusions presented here. In particular, studies into the convective instability of related boundary layers by the present authors [22,23] also use this approximation and all numerical results are verified by rigorous asymptotic investigations at high $R_L$. Furthermore, absolute instability is known to arise from inviscid modes which are observable in the purely inviscid and rigorous analysis of the Rayleigh equation obtained by neglected both streamline-curvature and viscous terms from the full system of perturbation equations. However, we do acknowledge that the results presented here will be subject to quantitative inaccuracies as a result of the approximation. A full discussion of the impact of the approximation is intended for a future paper in which the complementary asymptotic study will be presented.

Unfortunately, no experimental results for cones rotating in imposed axial flows are available for comparison at half-angles greater than $\psi = 15^\circ$. This means that quantitative comparisons of both the onset of spiral vortices (against convective instability) and the onset of turbulence (against absolute instability) cannot be made. Compiling the numerical codes for $\psi = 15^\circ$ would not be useful as this investigation is formulated to study crossflow instabilities, rather than the hypothesized Görtler modes on slender cones.

The results of this paper are restricted to local linear stability. The question of the global linear stability of the rotating disk was first investigated by Davies and Carpenter [32], who use a numerical

simulation to demonstrate that the global mode associated with the local absolute instability is damped. This has also been theoretically verified in the preliminary study of Garrett and Peake [21] for the boundary layers on disks and cones rotating in otherwise still fluids. It is therefore also likely to be the case when axial flow is incident on the rotating cone. Note, however, that this does not imply that absolute instability is not involved in transition. To see this, one must include nonlinearity: Pier et al. [33,34] have shown that a self-excited nonlinear global mode will always exist in the presence of a region of local absolute instability. This is in contrast to linear theory, since [21,32] have demonstrated that the region of local absolute instability on the disk is not sufficient to support an unstable linear global mode. Pier [35] has further shown that this nonlinear global mode can undergo secondary instability very close to the convective-absolute boundary, providing a possible route to turbulence. The global behavior needs to be investigated for the rotating-cone boundary layer both with and without an imposed axial flow.

In all papers in this series, an incompressible boundary layer has been assumed and methods from linear-stability theory applied. Although the assumption of incompressibility is reasonable for many aeroengine applications, it is not for the high-speed aerodynamic and CVD applications discussed in Sec. I. The investigations performed so far, although important in a theoretical context, must be considered as preliminary investigations with regard to such applications. Further work is therefore intended to study the effects of compressibility on the instability modes discussed. Work is also underway to clarify the transition mechanisms on slender cones.

## Acknowledgments

Z. Hussain wishes to acknowledge financial support from the School of Mathematics, University of Birmingham, and the Engineering and Physical Sciences Research Council (EPSRC). S. J. Garrett wishes to acknowledge study leave granted by the University of Leicester.

## References

[1] Reed, H. L., and Saric, W. S., "Stability of Three-Dimensional Boundary Layers," *Annual Review of Fluid Mechanics*, Vol. 21, 1989, pp. 235–284. doi:10.1146/annurev.fl.21.010189.001315

[2] Saric, W. S., Reed, H. L., and White, E. B., "Stability and Transition of Three-Dimensional Boundary Layers," *Annual Review of Fluid Mechanics*, Vol. 35, 2003, pp. 413–440. doi:10.1146/annurev.fluid.35.101101.161045

[3] Chen, K., and Mortazavi, A. R., "An Analytic Study of the Chemical Vapor Deposition (CVD) Processes in a Rotating Pedestal Reactor," *Journal of Crystal Growth*, Vol. 76, No. 1, 1986, pp. 199–208. doi:10.1016/0022-0248(86)90025-4

[4] Coltrin, M. E., Kee, R. J., and Evans, G. H., "A Mathematical Model of the Fluid Mechanics and Gas-Phase Chemistry in a Rotating Disk Chemical Vapor Deposition Reactor," *Journal of the Electrochemical Society*, Vol. 136, No. 3, 1989, pp. 819–829. doi:10.1149/1.2096750

[5] Vanka, S. P., Luo, G., and Glumac, N. G., "Parametric Effects on Thin Film Growth and Uniformity in an Atmospheric Pressure Impinging Jet CVD Reactor," *Journal of Crystal Growth*, Vol. 267, Nos. 1–2, 2004 pp. 22–34. doi:10.1016/j.jcrysgro.2004.03.039

[6] Kobayashi, R., and Arai, T., "Spiral Vortex Behaviour in Transition Region and Separation of Three-Dimensional Boundary Layers on Spheres Rotating in Axial Flow," *Laminar Turbulent Transition*, edited by D. Arnal and R. Michel, Springer, Berlin, 1990, pp. 551–557.

[7] Kobayashi, R., and Izumi, H., "Boundary-Layer Transition on a Rotating Cone in Still Fluid," *Journal of Fluid Mechanics*, Vol. 127, 1983, pp. 353–364. doi:10.1017/S0022112083002761

[8] Kobayashi, R., Kohama, Y., and Kurosawa, M., "Boundary-Layer Transition on a Rotating Cone in Axial Flow," *Journal of Fluid Mechanics*, Vol. 127, 1983, pp. 341–352. doi:10.1017/S002211208300275X

[9] Kohama, Y., "Behaviour of Spiral Vortices on a Rotating Cone in Axial Flow," *Acta Mechanica*, Vol. 51, Nos. 3–4, 1984, pp. 105–117. doi:10.1007/BF01177066

[10] Kohama, Y., "Flow Structures Formed by Axisymmetric Spinning Bodies," *AIAA Journal*, Vol. 23, No. 9, 1985, pp. 1445–1447. doi:10.2514/3.9105

[11] Kohama, Y., "Turbulent Transition Process of the Spiral Vortices Appearing in the Laminar Boundary Layer of a Rotating Cone," *Physicochemical Hydrodynamics: PCH*, Vol. 6, No. 5, 1985, pp. 659–669.

[12] Kobayashi, R., "Review: Laminar-to-Turbulent Transition of Three-Dimensional Boundary Layers on Rotating Bodies," *Journal of Fluids Engineering*, Vol. 116, No. 2, 1994, pp. 200–211. doi:10.1115/1.2910255

[13] Taniguchi, H., Kobayashi, R., and Fukunishi, Y., "Stability of the Boundary Layer on a Sphere Rotating in Still Fluid," *Acta Mechanica*, Vol. 129, Nos. 3–4, 1998, pp. 243–253. doi:10.1007/BF01176749

[14] Kobayashi, R., "Linear Stability Theory of Boundary Layer Along a Cone Rotating in Axial Flow," *Bulletin of the Japan Society of Mechanical Engineers*, Vol. 24, 1981, pp. 934–940.

[15] Kobayashi, R., Kohama, Y., and Kurosawa, M., "Boundary-Layer Transition on a Rotating Cone in Axial Flow," *Journal of Fluid Mechanics*, Vol. 127, 1983, pp. 341–352. doi:10.1017/S002211208300275X

[16] Salzberg, F., and Kezios, S. P., "Mass Transfer from a Rotating Cone in Axisymmetric Flow," *Journal of Heat Transfer*, Vol. 87, 1965, pp. 469–476.

[17] Garrett, S. J., "The Stability and Transition of the Boundary Layer on Rotating Bodies," Ph.D. Thesis, Cambridge Univ., Cambridge, England, U.K., 2002.

[18] Garrett, S. J., and Peake, N., "The Stability and Transition of the Boundary Layer on a Rotating Sphere," *Journal of Fluid Mechanics*, Vol. 456, 2002, pp. 199–217.

[19] Garrett, S. J., and Peake, N. "The Stability of the Boundary Layer on a Rotating Sphere in a Uniform Axial Flow," *European Journal of Mechanics, B/Fluids*, Vol. 23, No. 2, 2004, pp. 241–253. doi:10.1016/j.euromechflu.2003.08.004

[20] Garrett, S. J., and Peake, N., "The Absolute Instability of the Boundary Layer on a Rotating Cone," *European Journal of Mechanics, B/Fluids*, Vol. 26, No. 3, 2007, pp. 344–353. doi:10.1016/j.euromechflu.2006.08.002

[21] Garrett, S. J., and Peake, N., "On the Global Linear Stability of the Boundary Layer on Rotating Bodies," *Advances in Turbulence XI: Proceedings of the 11th EUROMECH European Turbulence Conference*, edited by J. M. L. M. Palma and A. Silva Lopes, Springer, Berlin, 2007, pp. 550–552.

[22] Garrett, S. J., Hussain, Z., and Stephen, S. O., "The Crossflow Instability of the Boundary Layer on a Rotating Cone," *Journal of Fluid Mechanics*, Vol. 622, 2009, pp. 209–232. doi:10.1017/S0022112008005181

[23] Hussain, Z., Garrett, S. J., and Stephen, S. O., "The Convective Instability of the Boundary Layer on a Rotating Disk in Axial Flow," *Physics of Fluids* (submitted for publication).

[24] Lingwood, R. J., "Absolute Instability of the Boundary Layer on a Rotating Disk," *Journal of Fluid Mechanics*, Vol. 299, 1995, pp. 17–33. doi:10.1017/S0022112095003405

[25] Lingwood, R. J., "An Experimental Study of Absolute Instability of the Rotating-Disk Boundary Layer Flow," *Journal of Fluid Mechanics*, Vol. 314, 1996, pp. 373–405. doi:10.1017/S0022112096000365

[26] Garrett, S. J., "Linear Growth Rates of Types I and II Convective Modes Within the Rotating-Cone Boundary Layer," *Fluid Dynamics Research*., Vol. 42, 2010, Paper 025504. doi:10.1088/0169-5983/42/2/025504

[27] Rosenhead, L., *Laminar Boundary Layers*, Oxford Univ. Press, Oxford, 1963.

[28] Evans, H., *Laminar Boundary Layer Theory*, Addison–Wesley, Reading, MA, 1968.

[29] Koh, J. C. Y., and Price, J. F., "Non-Similar Boundary-Layer Heat Transfer on a Rotating Cone in Axial Flow," *Journal of Heat Transfer* Vol. 89, 1967, pp. 139–145.

[30] Malik, M. R., "The Neutral Curve for Stationary Disturbances in Rotating-Disk Flow," *Journal of Fluid Mechanics*, Vol. 164, 1986, pp. 275–287. doi:10.1017/S0022112086002550

[31] Corke, T. C., and Knasiak, K. F., "Stationary Travelling Cross-Flow Mode Interactions on a Rotating Disk," *Journal of Fluid Mechanics*, Vol. 355, 1998, pp. 285–315. doi:10.1017/S0022112097007738

[32] Davies, C., and Carpenter, P. W., "Global Behaviour Corresponding to the Absolute Instability of the Rotating-Disk Boundary Layer," *Journal*

*of Fluid Mechanics*, Vol. 486, 2003, pp. 287–329. doi:10.1017/S0022112003004701

[33] Pier, B., Huerre, P., and Chomaz, J. M., "Bifurcation to Fully Nonlinear Synchronized Structures in Slowly Varying Media," *Physica D*, Vol. 148, Nos. 1–2, 2001, pp. 49–93. doi:10.1016/S0167-2789(00)00146-9

[34] Pier, B., and Huerre, P., "Nonlinear Self-Sustained Structures and Fronts in Spatially Developing Wake Flows," *Journal of Fluid Mechanics*, Vol. 435, 2001, pp. 359–381.

[35] Pier, B., "Fully Nonlinear Waves and Transition in the Boundary Layer over a Rotating Disk: Advances in Turbulence IX," *Proceedings of the 9th European Turbulence Conference*, edited by I. P. Castro, and P. E. Hancock, International Centre for Numerical Methods in Engineering, Barcelona, 2002, pp. 13–16.

A. Tumin
*Associate Editor*